

Subsurface warming derived by Argo floats during the 2022

Mediterranean marine heatwave

Annunziata Pirro¹, Riccardo Martellucci¹, Antonella Gallo¹, Elisabeth Kubin¹, Elena Mauri¹, Mélanie Juza², Giulio Notarstefano¹, Massimo Pacciaroni¹, Antonio Bussani¹, Milena Menna¹

¹National Institute of Oceanography and Applied Geophysics (OGS), Trieste, 34010, Italy

²Laboratory Balearic Islands Coastal Observing and Forecasting System (SOCIB), Palma, 07122, Spain

Correspondence to: Annunziata Pirro (apirro@ogs.it)

Abstract.

The Mediterranean marine heatwave (MHW) during the warm season (May-September) and the fall period (October-December) of 2022 is analyzed using Argo float in-situ observations in the upper 2000 m of depth. Five study regions (North Western Mediterranean, South Western Mediterranean, central Ionian Sea, Pelops Gyre and south Adriatic Pit) most affected by warming in different layers were selected and investigated. The primary goal is to provide insights into how the water column responds to the onset and progression of the MHW during the warming period, characterised by peak stratification and reduced vertical mixing. Additionally, this study aims to examine how the heat accumulated in the upper layers is redistributed to deep layers within regions with different dynamic characteristics through advection and/or mixing during the subsequent fall period.

Temperature anomaly profiles $T_a(z)$ computed for each area and for both periods were divided into three categories based on vertical heat penetration: Category 1 (shallow, 0-150 m), Category 2 (intermediate, 150-700 m) and Category 3 (deep, > 700 m). During the warm season, Category 1 profiles had a temperature anomaly near zero or slightly negative in a thin layer between 50 m and 150 m depth, while warming was observed in the 0-50 m layer and below the middle layer. Profiles characterized by greater vertical heat penetration (categories 2 and 3) were mainly in mesoscale or sub basin structures and showed the largest positive temperature anomaly in the surface and intermediate layers. All profile categories showed a warming between 200 and 800 m depth. This increase is roughly split, with half attributed to the impact of the 2022 MHW, and the other half linked to the ongoing long-term trend in ocean temperatures. During the fall period and in the layer below 200 m depth, the shape of the T_a profiles are similar for all sectors with the exception of the south Adriatic Pit, which depict a $+0.5^\circ\text{C}$ warming at 800 m depth.

29 The present work highlights the warming characteristics throughout the entire water column across different regions of the
30 Mediterranean Sea, and seeks to connect the impacts of the warm season on the cold period with oceanic dynamic processes,
31 such as dense water formation, upwelling or water column stratification. These regions are characterized by dynamic activities
32 (e.g. dense water formation, upwelling), therefore, any variation in these ocean processes can influence the thermohaline
33 circulation and, consequently, the climate system.
34

35 **Introduction**

36 Marine heatwaves (MHWs) are extreme ocean temperature events occurring over extended periods of time (Hobday et al.,
37 2016). Over the past decade the frequency of MHW events has increased by 50% (IPCC, 2023) as well as their duration and
38 magnitude (Oliver et al., 2018). They can affect small areas of coastline or span multiple ocean areas across latitudes with
39 significant impacts on ecosystems, coastal communities and economies (Wernberg et al., 2013; Garrabou et al., 2022; Dayan
40 et al., 2023).

41 Since the beginning of the 21st century the particularly rapid warming trend of the Mediterranean Sea surface layer has been
42 associated with a strong increase in MHWs events (Bensoussan et al., 2019, Ibrahim et al, 2021, Juza et al., 2022, Pastor and
43 Khodayar, 2022, Dayan et al., 2023). Several studies, mainly confined at the surface, have addressed this topic covering
44 different aspects of MHWs using satellite observations and model simulations. In particular, from basin to sub-regional scale,
45 previous works analyze MHWs drivers and indicators, estimate the frequency, the duration and intensity of MHWs, evaluate
46 their trend and assess the risk and the impacts on ecosystems (Darmaraki et al 2019, Galli et al., 2017, Garrabou et al., 2022,
47 Juza et al., 2022, Dayan et al., 2023, Martinez et al., 2023, Marullo et al., 2023, Pastor and Khodayar, Simon et al., 2023).
48 However, MHWs are not exclusively limited to the surface layer, but they can also propagate throughout the deeper layers of
49 the water column (Darmaraki et al., 2019, Shijian et al., 2021, Scannell H.A., 2020, Juza et al., 2022). This can cause negative
50 ecological consequences compromising the maintenance of the biodiversity, of the food and the regulation of air quality
51 (Garrabou et al., 2022; Holbrook et al., 2020; Santora et al., 2020; Smale et al., 2019; Schaeffer and Roughan, 2017; Lique
52 et al., 2016; Martín-Lopez et al., 2016; Mills et al., 2013). A recent work in the Mediterranean Sea shows that although MHWs
53 frequency is higher at the surface, their maximum intensity and duration is registered in the subsurface layers (Dayan et al.,
54 2023). Moreover, in-situ data collected in the tropical western Pacific Ocean show that the maximum intensity of almost every
55 MHW event is found in the subsurface layer, and many of the MHWs occurred even when no significant warming anomalies
56 are detected at the surface (Shijian et al., 2021). Using satellite data, Marullo et al. (2023) defined the occurrence of the event
57 in the Mediterranean Sea from May 2022 to spring 2023, with higher intensity in summer 2022 and in the band 0°-25° E.
58 Starting from this result, the present work analyzes the subsurface properties of the 2022 MHW in the upper 2000 m depth
59 using in-situ hydrographic Argo profiles (Product ref. no. 1, Table 1; Wong et al., 2020) collected during the period of highest

60 intensity (warm season, May-September) and in the period thereafter (cold season, October-December). Focusing on Marullo
61 et al. (2023) results and on the availability of Argo float profiles, five study areas were selected for our analysis (Figure 1(b)).
62

63

64

65

66

67

68

69

70

71

72

73

74

75

76

77

78

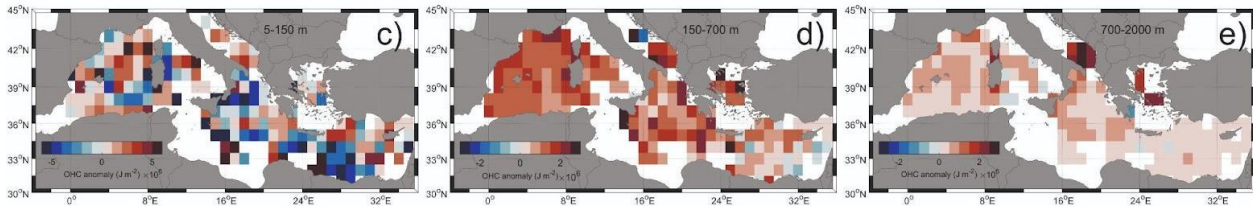
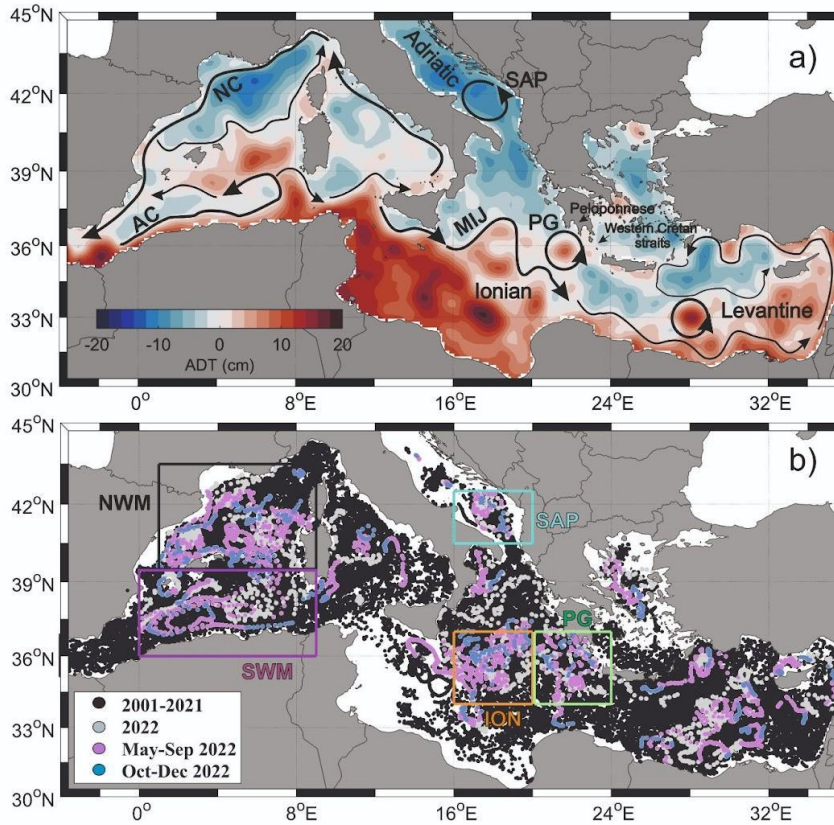
79

80

81

Product ref. no.	Product ID & type	Data access	Documentation
1	INSITU_MED_PHYBGCWAV_DISCRETE_MYNRT_013 _035; In-situ observations	EU Copernicus Marine Service Product, 2022a;	Quality Information Document (QUID): Wehde et al., (2022) Product User Manual (PUM): In Situ TAC partners (2022)
2	MEDSEA_MULTIYEAR_PHY_006_004; numerical models	EU Copernicus Marine Service Product, 2022b;	Quality Information Document (QUID): Escudier al., (2022) Product User Manual (PUM): Lecci et al., (2022)
3	SEALEVEL_EUR_PHY_L4_NRT_OBSERVATIONS_008 _060; satellite observations	EU Copernicus Marine Service Product, 2023;	Quality Information Document (QUID): Pujol al., (2023) Product User Manual (PUM): Pujol., (2022a)
4	SEADATANET_MedSea_climatology_V2; climatology	SEADATANET Product; 2022	Product Information Document (PIDoc): Simoncelli et al. (2020)

82 **Table 1: Product data used to perform the analysis of the present work**



84

85 **Figure1: (a) Absolute Dynamic Topography (colours) averaged for the warm season (May-September 2022) along with schematic**
 86 **pathways (black arrows) of the Algerian Current (AC), Northern Current (NC), Mid-Ionian Jet (MIJ), South Adriatic Pit (SAP)**
 87 **and Pelops Gyre (PG). (b) Argo floats position for the whole Mediterranean Sea. Black, magenta, cyan, orange and green boxes**
 88 **indicate the North West Mediterranean (NWM, 39.5-43.5°N; 1-9°E), South West Mediterranean (SWM, 36-39.5°N; 0-9°E), South**
 89 **Adriatic Pit (SAP, 40.5-42.5°N; 16-20°E), Ionian (ION, 34-37°N; 13-20°E) and Pelops Gyre (PG, 34-37°N; 20-24°E) areas,**
 90 **respectively. (c-e) 2022 Ocean Heat Content (OHC) anomaly estimated every meter with respect to the 2001-2018 FLOAT**
 91 **climatology period from Argo floats profiles in different layers (c, 5-150m), (d, 150-700), (e, 700-2000).**

92 Based on the vertical heat penetration (MHW depth, see Methods section), the temperature profiles collected in May-
 93 September 2022 from each study area were divided into three categories (shallow, intermediate and deep penetration) and the

94 median profile of temperature anomaly (\tilde{T}_a) was computed for each of them. Changes in the vertical temperature anomalies
95 were described and analyzed in relation to the ocean stratification, circulation and dynamics of each specific area. Lastly, this
96 study examines the properties of the water column during the fall period and speculates on its relationship with the dynamics
97 of the previous warm season's MHW. An estimation of the horizontal and vertical distribution of the Ocean Heat Content
98 (OHC) anomaly in 2022 was also performed in the whole Mediterranean Sea (Figures 1c-e).

99

100 **Methods**

101 The vertical propagation of the 2022 MHW in the Mediterranean Sea was investigated using temperature data collected by
102 Argo floats in the period 2001-2022 (Figure 1(b)). These data were collected and made freely available by the International
103 Argo Program (which is part of the Global Ocean Observing System (Argo 2023)) and by the national program Argo Italy that
104 contributes to it (<https://argo.ucsd.edu>, last access 23 April 2023; <https://www.ocean-ops.org>, last access 23 April 2023).

105 A comprehensive characterization of the event over the whole Mediterranean Sea was performed starting from the OHC
106 analysis. The OHC, defined as the total amount of heat absorbed and stored by the ocean, can be considered as a good indicator
107 for assessing the Earth's energy imbalance (Von Schuckmann et al., 2016). A float derived OHC climatology (OHC₂₀₀₁₋₂₀₁₈)
108 for the period 2001-2018 was estimated in 1° x 1° bins and in different layers (0-150 m, 150-700 m, 700-2000 m) using the
109 method of Kubin et al., 2023. Subsequently, Argo temperature data collected in 2022 were averaged on the same grid of
110 OHC₂₀₀₁₋₂₀₁₈ to compute the 2022 OHC (OHC₂₀₂₂). The OHCA₂₀₂₂ was then calculated as the difference between OHC₂₀₂₂ and
111 OHC₂₀₀₁₋₂₀₁₈ fields.

112 The five Mediterranean Sea regions most affected by surface warming (Figure 1b) were selected using the results of Marullo
113 et al. (2023) and considering the availability of float data. In these regions we analyzed the vertical penetration of the 2022
114 MHW signal in the water column both during the warm and cold season. The regions selected are: the North Western
115 Mediterranean (NWM), the South Western Mediterranean (SWM), the Ionian (ION), the Southern Adriatic Pit (SAP) and the
116 Pelops Gyre (PG) sectors.

117 The Temperature anomaly T_a at each depth z and for each profile was computed as:

$$T_a(z) = T(z) - \bar{T}(z), \quad (1)$$

118 for each sector. $T(z)$ is the 2022 temperature derived from Argo floats while $\bar{T}(z)$ is the climatological (1985-2018) averaged
119 temperature derived from the SeaDataCloud dataset (Product ref. no. 4, Table 1; SDC climatology). Specifically, the gridded
120 (0.125° x 0.125°) monthly climatological profiles were linearly interpolated in depth (every 10 m) and at the position of each
121 float profile. Moreover, to compare the 2022 MHW event with the averaged conditions estimated by floats in the selected

122 sectors, T_a profiles were also computed for the whole float dataset in the period 2001-2018 (FLOAT climatology). It's important
 123 to highlight that while this study utilizes the SDC climatology, the FLOAT climatology was utilized to facilitate a
 124 straightforward comparison with the OHC findings from Kubin et al. (2023). The time window used for the present work
 125 (May-September 2022) was chosen based on the latest European Space Agency specification
 126 (https://www.esa.int/Applications/Observing_the_Earth/Mediterranean_Sea_hit_by_marine_heatwave, last access 18
 127 February 2023) and on the estimations of Marullo et al. (2023). These indicate that the 2022 MHW developed in the second
 128 half of April in the northwest Mediterranean Sea and extended over the central Mediterranean into September. In this period,
 129 T_a profiles were quality controlled to remove any inconsistency (e.g. profiles with negative surface anomalies) and used to
 130 estimate the vertical propagation of the MHW (or MHW depth), following the method of Elzahaby and Schaeffer 2019. For
 131 each profile, the positive threshold depth (hereafter Z_N) is defined as the depth at which the first negative or 0 temperature
 132 anomaly occurred:

$$Z_N = \min (z(T_a(z) \leq 0)) , \quad (2)$$

133 Knowing Z_N , the vertical cumulative temperature anomaly (CT_a) defined as:

$$CT_a(Z_N) = \sum_{z=0}^{Z_N} T_a(z) \Delta z , \quad (3)$$

134 with $\Delta z = 10$ m, was computed for each profile from the surface ($z=0$) to the positive threshold depth ($z=Z_N$). To reduce the
 135 effect of the insignificant warming at depths per water profile, we define the MHW depth as the depth where a fraction ($\varepsilon=0.95$)
 136 of the cumulative T_a is reached:

$$MHWdepth = \max (z(CT_a(z) \leq \varepsilon \cdot CT_a(Z_N))) , \quad (4)$$

137 Based on MHW depth values, T_a profiles were then divided into three categories: Category 1 (shallow, 0-150 m), Category 2
 138 (intermediate, 150-700 m) and Category 3 (deep, > 700 m). It's noteworthy that within the SAP area, float profiles categorized
 139 as Category 2 and Category 3 consistently exhibit no negative temperature anomalies. However, they are classified into these
 140 categories based on their respective depths, shallower or deeper than 700 meters. Additionally, despite the limited number of
 141 profiles available in this region, they all fall within the cyclonic gyre. Hence, we are confident in considering them as
 142 representative of the entire SAP region. The median profile (\tilde{T}_a) for each category was obtained by spatially averaging all the
 143 available data in the different sectors in the warm period using 2022 and FLOAT climatology Argo data. Considering that the
 144 2022 MHW extends until the spring of 2023, (Marullo et al., 2023), the median profiles \tilde{T}_a for the fall period were also
 145 examined to investigate the accumulation of the heat in the water column. The mean T_a averaged in the surface, intermediate
 146 and deep layers as well as other additional information (number of profiles, MHW depth, max T_a and depth of max) are listed
 147 in Table 2.

148 Lastly, the Brunt-Väisälä frequency squared (N^2) for the year 2022 and in the upper 150 m depth was computed using monthly
149 averaged temperature and salinity Argo floats profiles for each sector in order to support the vertical heat penetration. The
150 same procedure was adopted to calculate the N^2 anomaly with respect to FLOAT climatology.

151

152

153

154

155

156

157

158

159

160

161

162

163

164

165

166

167

168

169

170

171

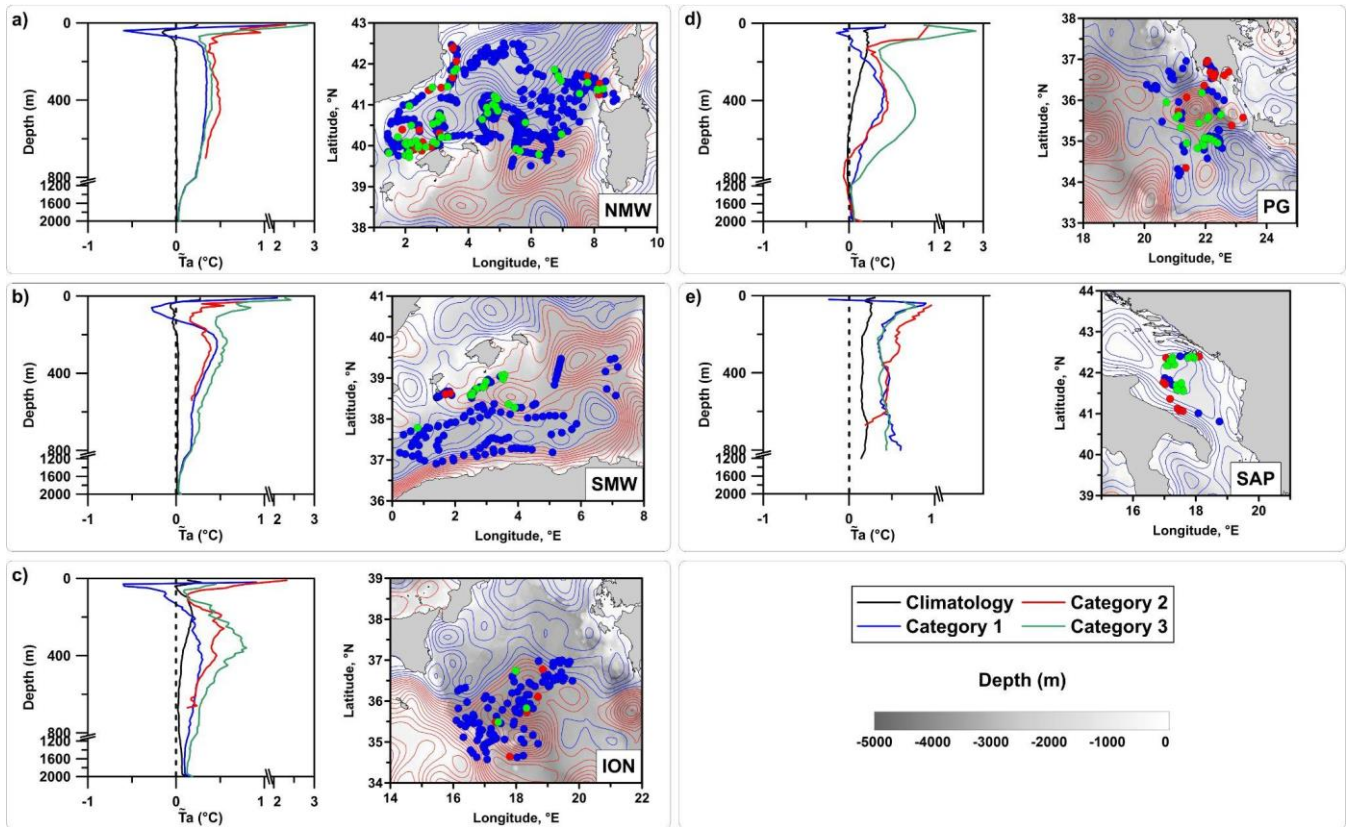
			Number of observations	MHW depth (m)	Temperature anomaly			averaged values		
					Surface (10 m)	Max	Depth of max (m)	0-150 m	150-700 m	700-2000 m
NWM	spring summer	C1	335	24,8	2,3	5,82	22,5	*0,28	0,32	0,097
		C2	16	571,9	2,2	5,48	50	0,32	0,4	NaN
		C3	43	1457,9	2,92	5,58	19,5	0,8	0,36	0,1
		clim	-	-	-	-	-	0,12	0,06	0,025
	fall	fall	306	-	-	-	-	0,66	0,33	0,11
		clim fall	-	-	-	-	-	0,08	0,07	0,04
SWM	spring summer	C1	159	25,6	2,13	5,79	22,5	0,19	0,33	0,088
		C2	5	630	1,83	5,46	24	0,43	0,3	NaN
		C3	27	1409,6	2,24	5,05	24,1	0,86	0,36	0,095
		clim	-	-	-	-	-	0,028	0,059	0,028
	fall	fall	148	-	-	-	-	0,18	0,31	0,11
		clim fall	-	-	-	-	-	0,1	0,05	0,02
ION	spring summer	C1	105	22,8	1,34	4,58	22,2	0,03	0,27	0,12
		C2	5	644	2,18	2,87	18	0,58	0,35	0,54
		C3	3	1383,4	1,39	1,97	20	0,47	0,54	0,15
		clim	-	-	-	-	-	0,071	0,091	0,057
	fall	fall	119	-	-	-	-	-0,21	0,26	0,12
		clim fall	-	-	-	-	-	-0,06	0,07	0,05
PG	spring summer	C1	50	37	1,34	3,82	41	0,15	0,32	0,03
		C2	15	553,4	0,95	6,15	47,3	0,97	0,34	0
		C3	20	1043,5	0,88	5,34	40	1,14	0,58	0,05
		clim	-	-	-	-	-	0,3	0,15	0,02
	fall	fall	70	-	-	-	-	-0,2	0,19	-0,02
		clim fall	-	-	-	-	-	0,27	0,13	0
SAP	spring summer	C1	9	32,2	1,18	3	24,5	0,57	0,39	0,66
		C2	10	411	1,95	7,25	27	1,04	0,46	NaN
		C3	17	945,3	0,88	4,36	78,8	0,72	0,4	0,59
		clim	-	-	-	-	-	0,3	0,21	0,21
	fall	fall	44	-	-	-	-	0,27	0,41	0,69
		clim fall	-	-	-	-	-	0,29	0,2	0,16

173 **Table 2: Characteristics of the 2022 MHW in Category 1 (C1), Category 2 (C2), Category 3 (C3): MHW depth, surface temperature**
174 **anomaly (Surface), maximum temperature anomaly (Max) and the depth where it occurs (Depth of max), mean temperature**
175 **anomaly for the surface (0-150 m), intermediate (150-700 m) and deep (700-2000 m) layers for each category and for the FLOAT**
176 **Climatology (clim).**

177

178 **Results and discussion**

179 In the surface layer, the OHCA_{2022} displayed inhomogeneous warming patterns, with positive anomalies areas adjacent to
180 others with strong negative anomalies (Figure 1(c)). Largest positive anomalies were observed in the West Mediterranean, in
181 the South Adriatic, in the eastern Ionian and northern Levantine basin. In the intermediate and deep layers the warming was
182 more homogeneous and widespread (Figures 1(d), 1(e)) where the majority of bins showed positive values of the OHCA_{2022}
183 and specifically, the western and central Mediterranean areas along with the Aegean Sea showed a more pronounced warming
184 compared to the Levantine basin, which exhibits a slight cooling in some bins of the central and eastern sectors. It can be stated
185 that half of this warming in the intermediate and deep layers is due to the 2022 MHW while the other half to the long-term
186 warming of the ocean. This consideration stems from comparing the current OHCA_{2022} with OHC trends defined by Kubin et
187 al. (2023). To perform this study, five regions (NWM, SWM, ION, SAP and PG; coloured boxes in Figure 1(b)) were selected.
188 This choice was motivated by the highest 2022 SST anomaly registered in the band 0 - 25° E (Marullo et al. 2023) and by the
189 availability of float data in both May-September and October-December 2022 periods. Figure 2 shows \tilde{T}_a profiles for the warm
190 season of each sector, for each MHW depth category and for the FLOAT climatology.



191

192

193

194

195

196

197

198

199

200

201

202

203

204

205

206

Figure 2: (left panels) Median profiles of temperature anomaly computed for each sector (NWM, SWM, ION, PG, SAP) and for the 2022 warm season (May-September) using Argo floats data with respect to the 1985-2018 SDC climatology dataset. Black lines highlight the FLOAT climatology profiles while blue, red and green profiles indicate shallow (0-150 m), intermediate (150-700 m) and deep (> 700m) categories, respectively. (right panels) Positive and negative contours of the Absolute Dynamic Topography with 1 cm spacing are displayed by red and blue lines while the coloured dots are associated to the floats position of each category.

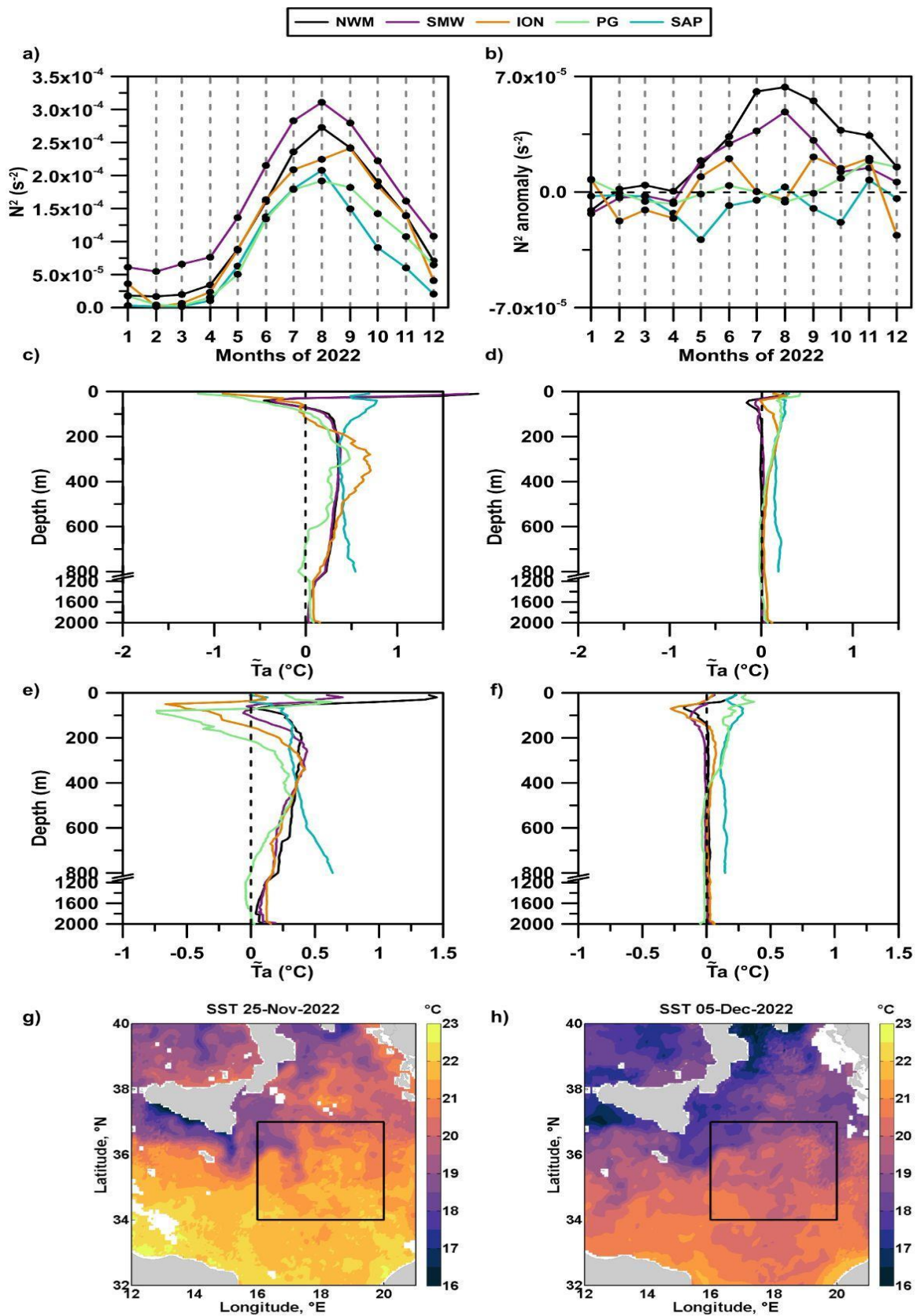
In the NWM and SWM sectors the circulation is strongly influenced by the presence of two intense and permanent currents (Figure 1(a)): the south-westward Northern Current (Poulain et al., 2012; Escudier et al., 2021) and the eastward along-slope Algerian Current (which transports waters of Atlantic origin in the upper water column (Poulain et al., 2021)) in the NWM and in the SWM, respectively. Therefore, float profiles were mainly located along the boundary of cyclonic circuits as highlighted by the Absolute Dynamic Topography (Product ref. no. 3, Table 1; (Figures 2(a), 2(b)). In the ION sector, float profiles were mainly distributed in the anticyclonic meander of the Mid-Ionian Jet (Figure 2(c)), a strong meandering current that together with the Atlantic-Ionian Stream (AIS), transports Atlantic Water from the western to the eastern Mediterranean Sea (Poulain et al., 2012, 2013; Menna et al., 2019a; Figure 1(a)). Although the NWM, SWM and ION sectors have different oceanographic characteristics, they showed a similar response to the 2022 MHW (Figure 2(a-c)). Most \bar{T}_a profiles belong to Category 1 and the mean MHW depth falls into the 20-25 m layer (Table 2). Profiles, characterized by shallow MHW

207 penetration (blue lines in Figures 2(a-c)), showed decreasing warming in the first 50 m with the maximum \tilde{T}_a close to the
208 surface (22.2-22.5 m; Table 2). The layer between 50 and 100 m depth showed a negative \tilde{T}_a with maxima of -0.65°C , -0.2°C
209 and -0.53°C at 50 m, 70 m and 40 m depth, in the NWM, SWM and ION sectors, respectively (Figures 2(a-c)). The median
210 profiles derived from the FLOAT climatology (black lines in Figure 2(a-c)) do not exhibit this negative anomaly (or only to
211 a very small extent), suggesting, therefore, a possible link between this behavior and the occurrence of the 2022 MHW. Below
212 100 m depth, the \tilde{T}_a becomes positive again with mean values of $\sim 0.3^\circ\text{C}$ in the intermediate layer and values lower than 0.12°C
213 in the deep layer. Profiles characterized by intermediate MHW penetration (red lines in Figures 2(a-c); MHW depth between
214 570 m and 650 m, Table 2) were located in coastal areas of the Western Mediterranean and in frontal zones in the ION sector,
215 and showed positive \tilde{T}_a throughout the water column, with values in the range of $0.3 - 0.6^\circ\text{C}$. Profiles, characterized by deep
216 MHW penetration (green lines in Figures 2(a-c); MHW depth ~ 1400 m, Table 2), showed the largest \tilde{T}_a in the surface layer
217 in the two sectors of the West Mediterranean ($> 0.8^\circ\text{C}$), while the ION sector depicted the largest anomalies in the intermediate
218 layer ($> 0.5^\circ\text{C}$). These results are consistent with the warming trend of the Western Mediterranean Sea over the last 15 years
219 of 0.09 ± 0.02 (0.03 ± 0.01) $^\circ\text{C}\cdot\text{yr}^{-1}$ for surface (intermediate) waters (Kubin et al., 2023).

220 The PG is located on the eastern side of the northern Ionian Sea, southwest of the Peloponnese coast (Figure 1(a)). It is a sub-
221 basin anticyclonic feature (diameter of ~ 120 km; Pinardi et al., 2015) which extends from the surface down to 800-1000 m
222 depth (Malanotte-Rizzoli et al., 1997; Kovacevic et al., 2015) and it is forced by the Etesian winds (Ayoub et al., 1998;
223 Mkhinini et al., 2014; Menna et al., 2021). In the late summer/fall the Etesian winds amplify their acceleration and the wind
224 shear in the region of the western Cretan straits (Mkhinini et al., 2014) therefore, larger anticyclonic vorticities are observed
225 during these months in the PG region (Menna et al., 2019a). In the sector PG, \tilde{T}_a profiles for the three categories showed
226 positive temperature anomalies in the first 800 m of the water column which coincides with the vertical extension of the gyre
227 itself (Figure 2(d)). Profiles that fall into Category 1 showed decreasing warming in the first 70 m, anomaly values close to
228 zero in the 70-150 m layer and increasing warming in the 150-400 m layer. The mean anomaly in the intermediate layer of
229 Category 1 is 0.3°C (Table 2). Category 2 profiles were retrieved mainly in the coastal area near the Peloponnese while
230 Category 3 profiles were found within the gyre area. Categories 2 and 3 showed strong warming in the surface layer (0.97°C
231 and 1.14°C , respectively), a mean warming in the range of $0.3-0.6^\circ\text{C}$ in the intermediate layer and no warming compared to
232 the SDC climatology was observed in the deep layer (Table 2).

233 The SAP is one of the sites of open ocean convection in the Mediterranean Sea, characterized by a complex thermohaline
234 circulation that influences the physical and biogeochemical properties of the dense waters formed in its interior and the strength
235 of winter convection (Martellucci et al., 2024; Di Biagio et al., 2023; Menna et al., 2022 OSR6; Pirro et al., 2022). This sector
236 showed positive temperature anomalies in all layers and in all categories (Figure 2(d)). Most profiles belong to Category 3
237 with a mean MHW depth of ~ 950 m and maximum \tilde{T}_a at ~ 80 m depth. The largest mean warming was observed in the surface
238 layer of each category ($0.6-1.04^\circ\text{C}$) followed by the deep layer, which had an exceptional warming of $\sim 0.6^\circ\text{C}$, and finally by
239 the intermediate layer, with a mean warming of $\sim 0.4^\circ\text{C}$ (Table 2).

240 All five sectors showed a larger warming than the FLOAT climatology with a mean temperature increase in the 2022 warm
241 season between 0.2° C and 0.8° C in response to the MHW event (Table 2). Some differences in warming observed among the
242 sectors are related to their peculiar hydrological and dynamical characteristics. During the warm season, the surface layer of
243 the NWM and SWM sectors and partially of the ION sector, was characterized by both larger stratifications and stratification
244 anomalies compared to the FLOAT climatology (Figures 3(a), 3(b)). Strong stratification prevents vertical heat penetration
245 causing negative \tilde{T}_a in the 50-100 m layer (Figure 2(a-c)). In the PG sector, warm season stratification anomaly was consistent
246 with climatology (Figure 3(b)), and vertical heat penetration was closely related to the gyre dynamics. In the SAP sector,
247 stratification during the warm period was lower than climatology suggesting an instability of the water column and therefore
248 the transport of the vertical heat to the deep layers. The median of all profiles available in 2022 warm season, when not
249 categorized, closely aligns with the median of profiles in category C1 (Figures 3(c), 3(d)). This condition arises because
250 category C1 consistently boasts the highest number of profiles across various sectors.



252 **Figure3: (a) Monthly averaged Brunt - Väisälä frequency squared (N^2) computed in the surface layer (0-150 m) using 2022 Argo**
253 **float data. (b) Monthly averaged Brunt Brunt—Väisälä frequency squared anomaly (N^2 anomaly) computed in the surface layer**
254 **with respect to the FLOAT climatology. (c) Median Temperature anomaly ($^{\circ}\text{C}$) computed in the warm season (May - September)**
255 **from Argo floats profiles in 2022 and (d) in 2001-2018 with respect to the SDC climatology. (e) Median Temperature anomaly ($^{\circ}\text{C}$)**
256 **computed in fall period (October - December) from Argo floats profiles in 2022 and (e) in 2001-2018 with respect to the SDC**
257 **climatology). (g) Daily Sea Surface Temperature ($^{\circ}\text{C}$) in the ION sector (black box) for late November and (h) early December 2022.**

258 Larger warming of the water column was observed in fall 2022 compared to the SDC climatology in all sectors, except for the
259 surface layer of the ION and PG sectors (Figure 3e). The stronger warm season stratification observed in the NWM and SWM
260 sectors (Figures 3(a), 3(b)) corresponds to enhanced vertical heat propagation in the surface and intermediate layers in fall
261 2022 (Figure 3(e), Table 2). Negative \tilde{T}_a values in the surface layer of the ION sector were attributed to an upwelling event
262 along the southern coast of Sicily between November and December 2022 as shown by the Sea Surface Temperature (Product
263 ref. no. 2, Table 1; (Figures 3(g), 3(h)). The northern part of the Sicily Channel is an area of strong eddy kinetic energy (Poulain
264 et al., 2012) influenced by Ekman transport and advection of waters from the western to the eastern Mediterranean (Molcard
265 et al., 2002; Falcini et al., 2015; Schroeder et al., 2017; Menna et al., 2019b). The cold waters upwelled off the southern coast
266 of Sicily in November 2022 (Figure 3(g)) were advected to the Ionian Sea through the Atlantic-Ionian Stream and the Mid-
267 Ionian Jet pathways (Figure 1(a)), and gradually cooling the waters in the ION sector (Figure 3(h)). The negative anomaly in
268 the surface layer of the ION sector is not limited only to 2022 but is a permanent characteristic of the area related to the
269 upwelling phenomena, as confirmed by the \tilde{T}_a profile derived from the FLOAT climatology (orange line in Figure 3(f)) and
270 by trends of the OHC anomaly estimated by Dayan et al. (2023) over the period 1987-2019. Negative \tilde{T}_a values in the PG
271 sector were imputable to the typical downwelling process of this region associated with the gyre dynamics. The downwelling
272 contributed to the vertical propagation of the 2022 MHW, with a strong spring-summer warming in the first 800 m of the water
273 column (Figure 2d), keeping the stratification values similar to the FLOAT climatology (no significant increases of N^2 anomaly
274 was registered due to the 2022 heatwave; Figure 3(b)). In this way, fall cooling can penetrate deep into the water column
275 causing, therefore, negative \tilde{T}_a values in the surface layer (Figure 3(e).; Table 2).

276 In recent years, the SAP is experiencing a significant temperature increase in the deep layer (trend of $\sim 0.06^{\circ}\text{C}\cdot\text{yr}^{-1}$ in the
277 2013-2020 period according to Kubin et al., 2023) and salinity in the surface and intermediate layers (Martellucci et al., 2024;
278 Menna et al., 2022 OSR6; Mihanovich et al., 2021) with potential future effects on the whole thermohaline cell of the Eastern
279 Mediterranean. It is of general understanding that convection sites contribute to the propagation of the MHWs signal from the
280 surface to the subsurface interior of the water column (Dayan et al., 2023; Kubin et al., 2023) but specific analysis at the local
281 scale are not yet available (Juza et al., 2022). Our results show a fair significant warming of the SAP in both spring-summer
282 (Figures 2(e) and 3(c)) and fall (light blue line in Figure 3(f)) 2022 and a significant positive anomaly of FLOAT climatology
283 compared to SDC one (black line in Figure 2(e) and light blue line in Figure 3(f)). In fall, largest \tilde{T}_a in the SAP were observed
284 in the deep layer ($\sim 0.69^{\circ}\text{C}$); Table 2, Figure 3(e)). Mean profiles derived from Float Climatology (black line in Figure 2(e))

285 and light blue line in Figure 3(f)) showed positive values compared to SDC one, confirming the warming trend throughout the
286 water column over the past decade. Beyond the impact of the global warming of the Mediterranean Sea, the 2022 MHW leads
287 to an additional heating in the SAP, which is transferred to the deeper layers favored by dynamical features of this area.
288 This study aims to characterize the 2022 MHW in the subsurface layers, and attempts to explain the mechanisms that drive the
289 heat penetration to deep layers. However, further and more detailed investigations are needed to better support this last
290 conclusion. We show that the effects of the 2022 MHW are felt in all layers of the Mediterranean Sea with vertical heat
291 propagation extending from the surface to ~1500 m depth. In the surface layer, heat penetration and storage are related to the
292 strength of the stratification and/or advection from adjacent regions. In contrast, the transport and the storage of heat in the
293 intermediate and deep layers are closely linked to the dynamics of each area. These considerations are in line with the findings
294 of Elzahaby et al. (2021) and Zhang et al. (2023), who noted that shallower MHWs are primarily influenced by surface air-sea
295 fluxes, whereas deeper MHWs are predominantly driven by advection, manifesting distinct dynamics across various oceanic
296 regions.

297 In the western Mediterranean and western Ionian Sea sectors, heat is mainly stored in the surface layer (shallow MHW depths
298 and stronger stratification) so that this layer is significantly warmer than the climatology even during the following fall.
299 Although deep MHW penetration in these regions is limited to coastal and frontal/eddies zones, it reaches the higher MHW
300 depth estimated during the event. Sectors characterized by specific dynamics conditions (downwelling, convection) quickly
301 distribute the heat in the water column even during the event. Intermediate layers exhibit comparable heating both during and
302 after the MHW event, implying that heat can be stored there for extended periods and can be regarded as a long-term signal.
303 The warming signal in the intermediate and deep layers could also be influenced by heat advection from adjacent basins
304 however, we are aware that this topic needs to be studied in more detail in the future. In this context, the use of two
305 climatologies and the cumulative anomaly threshold in the present analysis should have eliminated most of the signal
306 associated with the ocean warming trend and advection therefore, the additional warming registered in spring-summer 2022
307 compared to the FLOAT climatology can be attributed to the effects of the 2022 MHW along the entire water column. Further
308 studies are needed to investigate the effects that this warming may have on the physical and biological oceanic processes with
309 implications on the thermohaline circulation of the entire Mediterranean Sea.

310

311

312 Competing interests. The contact author has declared that neither they nor their co-authors have any competing interests.

313

314 Author contributions. Conceptualization of the study was done by AP, MM and RM. AP and MM prepared the original
315 manuscript. AP, MM, RM, EM, AG, GN, EK and MJ reviewed and edited the manuscript. AP, MM and RM created the
316 methodology. AP, MM, RM and EK created the codes and performed the formal analysis. AP, MM, RM conducted the
317 investigation. AG, AB and MP curated the data. EM was in charge of Argo-Italy infrastructure management and funding
318 acquisition. All authors have read and agreed to the published version of the paper.

319

320 Code/data availability. The codes and data are available upon request to apirro@ogs.it

321 **References**

322 Argo: Argo float data and metadata from Global Data Assembly Centre (Argo GDAC). SEANOE.
323 <https://doi.org/10.17882/42182>, 2023.

324 Ayoub, N., Le Traon, P.-Y., and De Mey, P.: A description of the Mediterranean surface variable circulation from combined
325 ERS-1 and TOPEX/POSEIDON altimetric data. *J.Mar. Syst.* 18, 3–40, [https://doi.org/10.1016/S0924-7963\(98\)80004-3](https://doi.org/10.1016/S0924-7963(98)80004-3), 1998.

326 Bensoussan, N., Chiggiato, J., Buongiorno Nardelli, B., Pisano, A. and Garrabou, J.: Insights on 2017 marine heat waves in
327 the Mediterranean sea. *J. Oper. Ocean.*, 12 (1), s26–s30, <https://doi.org/10.1080/1755876X.2019.163307>, 2019.

328 Darmaraki, S., Somot, S., Sevault, F. and Nabat, P.: Past variability of Mediterranean Sea marine heatwaves, *Geophys. Res.*
329 *Let.*, 46 (16), 9813–9823, <https://doi.org/10.1029/2019GL082933>, 2019.

330 Dayan, H., McAdam, R., Juza, M., Masina, S. and Speich, S.: Marine heat waves in the Mediterranean Sea: An assessment
331 from the surface to the subsurface to meet national needs. *Front. Mar. Sci.*, <https://doi.org/10.1045138>,
332 1010.3389/fmars.2023.1045138, 2023.

333 Di Biagio, V., Martellucci, R., Menna, M., Teruzzi, A., Amadio, C., Mauri, E., & Cossarini, G.: Dissolved oxygen as an
334 indicator of multiple drivers of the marine ecosystem: the southern Adriatic Sea case study. *State of the Planet*, 1, 1-13,
335 <https://doi.org/10.5194/sp-1-osr7-10-2023>, 2023.

336 Elzahaby, Y. and Schaffer, A.: Observational insight into the subsurface anomalies of marine heatwaves. *Front. Mar. Sci.*,
337 6:745, <https://doi.org/10.3389/fmars.2019.00745>, 2019.

338 Elzahaby, Y., Schaeffer, A., Roughan, M., & Delaux, S.: Oceanic circulation drives the deepest and longest marine heatwaves
339 in the East Australian Current system. *Geoph. Res. Lett.*, 48(17), <https://doi.org/10.1029/2021GL094785>, 2021.

340 Escudier, R., Clementi, E., Cipollone, A., Pistoia, J., Drudi, M., Grandi, A., Lyubartsev, V., Lecci, R., Aydogdu, A., Delrosso,
341 D., Omar, M., Masina, S., Coppini, G. and Pinardi, N.: A High Resolution Reanalysis for the Mediterranean Sea. *Front. Earth*
342 *Sci.*, 9:702285, <https://doi.org/10.3389/feart.2021.702285>, 2021.

343 Falcini, F. and Salusti, E.: Friction and mixing effects on potential vorticity for bottom current crossing a marine strait: an
344 application to the Sicily Channel (central Mediterranean Sea). *Ocean Sci.*, 11, 391–403, [https://doi.org/10.5194/os-11-391-](https://doi.org/10.5194/os-11-391-2015)
345 2015, 2015.

- 346 Galli, G., Solidoro C., and Lovato T.: Marine heat waves hazard 3D maps and the risk for low motility organisms in a warming
347 Mediterranean Sea. *Front. Mar. Sci.*, 4: 136, <https://doi.org/10.3389/fmars.2017.00136>, 2017.
- 348 Garrabou, J. et al.: Marine heatwaves drive recurrent mass mortalities in the Mediterranean Sea. *Global Change Biology*,
349 <https://doi.org/10.1111/gcb.16301>, 2022
- 350 Hobday, A. J., Alexander, L. V., Perkins, S. E., Smale, D. A., Straub, S. C., Oliver, E. C., Benthuyesen, J. A., Burrows, M. T.,
351 Donat, G. M., Feng, M., Holbrook, N., J., Moore, P. J., Scannel, H. A., Gupta, A. S. and Wernberg T.: A hierarchical approach
352 to defining marine heatwaves. *Prog. Oceanogr.* 141, 227–238, <https://doi.org/10.1016/j.pocean.2015.12.014>, 2016.
- 353 Holbrook, N. J., Gupta, A. S., Oliver, E. C., Hobday, A. J., Benthuyesen, J. A., Scannell, H. A., et al.: Keeping pace with marine
354 heatwaves. *Nat. Rev. Earth Env.*, 1 (9), 482– 493, <https://doi.org/10.1038/s43017-020-0068-4>, 2020.
- 355 Ibrahim, O., Mohamed, B., and Nagy, H.: Spatial variability and trends of marine heat waves in the Eastern Mediterranean
356 Sea over 39 years. *J. Mar. Sci. Eng.*, 9 (6), 643, <https://doi.org/10.3390/jmse9060643>, 2021.
- 357 Intergovernmental Panel on Climate Change (IPCC): Summary for Policymakers. In: *Climate Change 2023, Synthesis Report*,
358 Summary for Policymakers, Core Writing Team, Lee, H. and Romero, J., 36,
359 https://www.ipcc.ch/report/ar6/syr/downloads/report/IPCC_AR6_SYR_SPM.pdf, 2023.
- 360 Juzá, M., Fernández-Mora, A., and Tintoré, J.: Sub-Regional marine heat waves in the Mediterranean Sea from observations:
361 long-term surface changes, subsurface and coastal responses. *Front. Mar. Sci.* 9, 785771, <https://doi.org/10.3389/fmars.2022.785771>, 2022.
- 363 Kovačević, V., Ursella, L., Gačić, M., Notarstefano, G., Menna, M., Bensi, M., and Poulain, P.-M.: On the Ionian thermohaline
364 properties and circulation in 2010–2013 as measured by Argo floats. *Acta Adriat.*, 56(1): 97 - 114, 2015.
- 365 Kubin, E., Menna, M., Mauri, E., Notarstefano, G., Mieruch, S., and Poulain, P.-M.: Heat content and temperature trends in
366 the Mediterranean Sea as derived from Argo float data. *Front. Mar. Sci.* 10, 1271638,
367 <https://doi.org/10.3389/fmars.2023.1271638>, 2023.
- 368 Liqueste, C., Piroddi, C., Macias, D., Druon, J. N., and Zulian, G.: Ecosystem services sustainability in the Mediterranean Sea:
369 assessment of status and trends using multiple modelling approaches. *Sci. Rep.* 6 (1), 1–14, <https://doi.org/10.1038/srep34162>,
370 2016.
- 371 Malanotte-Rizzoli, P., Manca, B. B., Ribera D’Alcalà, M., Theocharis, A., Bergamasco, A., Bregant, D., Budillon, G.,
372 Civitarese, G., Georgoupoulos, D., Michelato A., Sansone, E., Scarazzato, P., Souvermezoglou, E.: A synthesis of
373 the Ionian Sea hydrography, circulation and water masses pathways during POEM-Phase I. *Prog. Oceanogr.*, 39, 153–204,
374 [https://doi.org/10.1016/S0079-6611\(97\)00013-X](https://doi.org/10.1016/S0079-6611(97)00013-X), 1997.
- 375 Martín-Lopez, B., Oteros-Rozas, E., Cohen-Shacham, E., Santos-Martín, F., Nieto-Romero, M., Carvalho-Santos, C., et al.:
376 Ecosystem services supplied by mediterranean basin ecosystems, in *Routledge handbook of ecosystem services*. Eds. M.
377 Potschin, R. Haines-Young, R. Fish and R. K. Turner (London: Routledge), 405–414, 2016.
- 378 Martellucci, R., Menna, M., Mauri, E., Pirro, A., Gerin, R., de Mendoza, F. P., ... & Poulain, P. M.: Recent changes of the
379 dissolved oxygen distribution in the deep convection cell of the southern Adriatic Sea. *Journal of marine systems*, 245, 103988,
380 2024.

- 381 Martínez, J., Leonelli, F. E., García-Ladona, E., Garrabou, J., Kersting, D., Bensoussan, N., & Pisano, A.: Evolution of marine
382 heatwaves in warming seas: the Mediterranean Sea case study. *Front. Mar. Sci.*, <https://doi.org/10.3389/fmars.2023.1193164>,
383 2023.
- 384 Marullo, S., Serva, F., Iacono, R., Napolitano, E., di Sarra, A., Meloni, D., ... & Santoleri, R.: Record-breaking persistence of
385 the 2022/23 marine heatwave in the Mediterranean Sea. *Env. Res. Lett.*, 18(11), 114041, <https://doi.org/10.1088/1748-9326/ad02ae>, 2023.
- 387 Menna, M., Suarez, N. R., Civitarese, G., Gačić, M., Rubino, A., and Poulain, P. M.; Decadal variations of circulation in the
388 Central Mediterranean and its interactions with mesoscale gyres. *Deep Sea Res. II*, 164, 14-24,
389 <https://doi.org/10.1016/j.dsr2.2019.02.004>, 2019a.
- 390 Menna, M., Poulain, P. M., Ciani, D., Doglioli, A., Notarstefano, G., Gerin, R., Rio, M. H. Santoleri, R., Gauci, A. and Drago,
391 A.: New Insights of the Sicily Channel and Southern Tyrrhenian Sea Variability. *Water*, 11, 1355,
392 <https://doi.org/10.3390/w11071355>, 2019b.
- 393 Menna, M., Gerin, R., Notarstefano, G., Mauri, E., Bussani, A., Pacciaroni, M., and Poulain, P. M.: On the circulation and
394 thermohaline properties of the Eastern Mediterranean Sea. *Fron. Mar. Sci.*, 8, 671469,
395 <https://doi.org/10.3389/fmars.2021.6714692>, 2021.
- 396 Menna, M., Martellucci, R., Notarstefano, G., Mauri, E., Gerin, R., Pacciaroni, M., Bussani, A., Pirro, A., Poulain, P. M.:
397 Record-breaking high salinity in the South Adriatic Pit in 2020. *J. Oper. Oceanogr.*, s199-s205,
398 <https://doi.org/10.1080/1755876X.2022.2095169>, 2022.
- 399 Mihanović, H., Vilibić, I., Šepić, J., Matić, F., Ljubešić, Z., Mauri, E., Gerin, R.: Observation, preconditioning and recurrence
400 of exceptionally high salinities in the Adriatic Sea. *Front. Mar. Sci.*, 8:834. <https://doi.org/10.3389/fmars.2021.672210>, 2021.
- 401 Mills, K. E., Pershing, A. J., Brown, C. J., Chen, Y., Chiang, F. S., Holland, D. S., et al.: Fisheries management in a changing
402 climate: lessons from the 2012 ocean heat wave in the Northwest Atlantic. *Oceanography* 26 (2), 191–195,
403 <https://doi.org/10.5670/oceanog.2013.27>, 2013.
- 404 Molcard, A., Gervasio, L., Gria, A., Gasparini, G. P., Mortier, L., Ozgokmen, T. M.: Numerical investigation of the Sicily
405 Channel dynamics: density currents and water mass advection. *J. Mar. Syst.*, 36, 219–238, [https://doi.org/10.1016/S0924-7963\(02\)00188-4](https://doi.org/10.1016/S0924-7963(02)00188-4), 2002.
- 407 Mkhinini, N., Coimbra, A. L. S., Stegner, A., Arsouze, T., Taupier-Letage, I., and Beranger, K.: Long-lived mesoscale eddies
408 in the Eastern Mediterranean Sea: analysis of 20 years of AVISO geostrophic velocities. *J. Geophys. Res. Oceans* 119, 8603–
409 8626, <https://doi.org/10.1002/2014JC010176>, 2014.
- 410 Oliver, E. C., Donat, M. G., Burrows, M. T., Moore, P. J., Smale, D. A., Alexander, L. V., Benthuisen, J. A., Feng, M., Gupta,
411 A. S., Hobday, A. J., Holbrook, N. J., Perkins-Kirkpatrick, S. E., Scannell, H. E., Straub, S. C. and Wernberg, T.: Longer and
412 more frequent marine heatwaves over the past century. *Nat. Commun.*, 9:1324, <https://doi.org/10.1038/s41467-018-03732-9>,
413 2018.
- 414 Pinardi, N., Zavatarelli, M., Adani, M., Coppini, G., Fratianni, C., Oddo, P., Simoncelli, S., Tonani, M., Lyubartsev, V.:
415 Mediterranean Sea large-scale low-frequency ocean variability and water mass formation rates from 1987 to 2007: a
416 retrospective analysis. *Prog. Oceanogr.* 132, 318–332, <https://doi.org/10.1016/j.pocean.2013.11.003>, 2015.
- 417 Pastor, F., & Khodayar, S.: Marine heat waves: Characterizing a major climate impact in the Mediterranean. *Science of The*
418 *Total Env.*, 861, 160621, <https://doi.org/10.1016/j.scitotenv.2022.160621>, 2023.

- 419 Pirro, A., Mauri, E., Gerin, R., Martellucci, R., Zuppelli, P. and Poulain, P. M.: New insights on the formation and breaking
420 mechanism of convective cyclonic cones in the South Adriatic Pit during winter 2018. *J. Phys. Oceanogr.*, 52(9), 2049-2068,
421 <https://doi.org/10.1175/JPO-D-21-0108.1>, 2022.
- 422 Poulain, P. M., Menna, M., and Mauri, E.: Surface geostrophic circulation of the Mediterranean Sea derived from drifter and
423 satellite altimeter data. *J. Phys. Oceanogr.*, 42(6), 973-990, <https://doi.org/10.1175/JPO-D-11-0159.1>, 2012.
- 424 Poulain, P. M., Bussani, A., Gerin, R., Jungwirth, R., Mauri, E., Menna, M. and Notarstefano, G.: Mediterranean surface
425 currents measured with drifters: From basin to subinertial scales. *Oceanography* 26 (1), 38–47,
426 <https://doi.org/10.5670/oceanog.2013.03>, 2013.
- 427 Poulain, P. M., Centurioni, L., Özgökmen, T., Tarry, D., Pascual, A., Ruiz, S., Mauri, E., Menna, M. and Notarstefano, G.: On
428 the structure and kinematics of an Algerian Eddy in the southwestern Mediterranean Sea. *Rem. Sens.*, 13(15), 3039,
429 <https://doi.org/10.3390/rs13153039>, 2021.
- 430 Pastor, F. and Khodayar, S.: Marine heat waves: Characterizing a major climate impact in the Mediterranean. *Sci. Tot. Env.*,
431 861, 160621, <https://doi.org/10.1016/j.scitotenv.2022.160621>, 2022.
- 432 Santora, J. A., Mantua, N. J., Schroeder, I. D., Field, J. C., Hazen, E. L., Bograd, S. J., et al.: Habitat compression and ecosystem
433 shifts as potential links between marine heatwave and record whale entanglements. *Nat. Commun.* 11 (1), 1–12,
434 <https://doi.org/10.1038/s41467-019-14215-w>, 2020.
- 435 Scannell, H. A., Johnson, G. C., Thompson, L., Lyman, J. M., and Riser, S. C.: Subsurface evolution and persistence of marine
436 heatwaves in the Northeast Pacific. *Geophys. Res. Lett.*, 47, e2020GL090548, <https://doi.org/10.1029/2020GL090548>, 2020.
- 437
- 438 Schaeffer, A., and Roughan, M.: Subsurface intensification of marine heatwaves off southeastern Australia: the role of
439 stratification and local winds. *Geoph. Res. Lett.*, 44 (10), 5025–5033, <https://doi.org/10.1002/2017gl073714>, 2017.
- 440 Schroeder, K., Chiggiato, J., Josey, S.A., Borghini, M., Aracri, S., Sparnocchia, S.: Rapid response to climate change in a
441 marginal sea. *Sci. Rep.*, 7, 4065, <https://doi.org/10.1038/s41598-017-04455-5>, 2017.
- 442 Shijian H., S., Li, S., Zhang, Y., Guan, C., Du, Y., Feng, M., Anodo, K., Wang, F., Schiller, A. and Hu, D.: Observed strong
443 subsurface marine heatwaves in the tropical western Pacific Ocean. *Env. Res. Lett.*, 16(10), 104024,16 104024,
444 <https://doi.org/10.1088/1748-9326/ac26f2>, 2021.
- 445 Simon, A., Pires, C., Frölicher, T. L., & Russo, A.: Long-term warming and interannual variability contributions' to marine
446 heatwaves in the Mediterranean. *Weather and Climate Extremes*, 42, 100619, <https://doi.org/10.1016/j.wace.2023.100619>,
447 2023.
- 448 Smale, D. A., Wernberg, T., Oliver, E. C., Thomsen, M., Harvey, B. P., Straub, S. C., et al.: Marine heatwaves threaten global
449 biodiversity and the provision of ecosystem services. *Nat. Climate Change*, 9 (4), 306–312, [https://doi.org/10.1038/s41558-](https://doi.org/10.1038/s41558-019-0412-1)
450 [019-0412-1](https://doi.org/10.1038/s41558-019-0412-1), 2019.
- 451 Von Schuckmann, K., Palmer, M. D., Trenberth, K. E., Cazenave, A., Chambers, D., Champollion, N., Hansen, J., Josey, S.
452 A., Loeb, N., Mathieu, P. P., Meyssignac, B. and Wild, M.: An imperative to monitor earth's energy imbalance. *Nat. Clim.*
453 *Change*, 6 (2), 138–144, [doi:10.1038/nclimate2876](https://doi.org/10.1038/nclimate2876), 2016.

- 454 Wernberg, T., Smale, D. A., Tuya, F., Thomsen, M. S., Langlois, T. J., De Bettignies, T., Bennet, S. and Rousseaux, C. S.: An
455 extreme climatic event alters marine ecosystem structure in a global biodiversity hotspot. *Nat. Clim. Change*, 3, 78–82,
456 <https://doi.org/10.1038/nclimate1627>, 2013.
- 457 Wong, A. P., Wijffels, S. E., Riser, S. C., Pouliquen, S., Hosoda, S., Roemmich, D., et al.: Argo Data 1999–2019: Two Million
458 Temperature-Salinity Profiles and Subsurface Velocity Observations From a Global Array of Profiling Floats. *Front. Mar. Sci.*,
459 7(700), <https://doi.org/10.3389/fmars.2020.00700>, 2020.
- 460 Zhang, Y., Du, Y., Feng, M., & Hobday, A. J.: Vertical structures of marine heatwaves. *Nature Communications*, 14(1), 6483,
461 <https://doi.org/10.1038/s41467-023-42219-0>, 2023.

462

463 **References for Table 1**

464 Product ref no.1

465 EU Copernicus Marine Service Product: Mediterranean Sea- In-Situ Near Real Time Observations, Mercator Ocean
466 International [data set], <https://doi.org/10.48670/moi-00044>, 2022.

467 H. Wehde, K. V. Schuckmann, S. Pouliquen, A. Grouazel, T Bartolome, J Tintore, M. De Alfonso Alonso-Munoyerro, T.
468 Carval, V. Racapé and the INSTAC team: EU Copernicus Marine Service Quality Information Document for Mediterranean
469 Sea- In-Situ Near Real Time Observations, INSITU_MED_PHYBGCWAV_DISCRETE_MYNRT_013_035, Issue 2.2,
470 Mercator Ocean International, [https://catalogue.marine.copernicus.eu/documents/QUID/CMEMS-INS-QUID-013-030-
471 036.pdf](https://catalogue.marine.copernicus.eu/documents/QUID/CMEMS-INS-QUID-013-030-036.pdf), last access: 19 May 2023, 2022.

472 In Situ TAC partners: EU Copernicus Marine Service Product User Manual for Mediterranean Sea- In-Situ Near Real Time
473 Observations, INSITU_MED_PHYBGCWAV_DISCRETE_MYNRT_013_035, Issue 1.14, Mercator Ocean International,
474 <https://catalogue.marine.copernicus.eu/documents/PUM/CMEMS-INS-PUM-013-030-036.pdf>, last access: 19 May 2023,
475 2022.

476 Product ref no.2

477 EU Copernicus Marine Service Product: Mediterranean Sea Physics Reanalysis, Mercator Ocean International [data set],
478 https://doi.org/10.25423/CMCC/MEDSEA_MULTIYEAR_PHY_006_004_E3R1I, 2022.

479 R. Escudier, E. Clementi, T. Nigam, A. Aydogdu, E. Fini, J. Pistoia, A. Grandi, P. Miraglio: EU Copernicus Marine Service
480 Quality Information Document for Mediterranean Sea Physics Reanalysis, MEDSEA_MULTIYEAR_PHY_006_004, Issue
481 2.3, Mercator Ocean International, [https://catalogue.marine.copernicus.eu/documents/QUID/CMEMS-MED-QUID-006-
482 004.pdf](https://catalogue.marine.copernicus.eu/documents/QUID/CMEMS-MED-QUID-006-004.pdf), last access: 19 May 2023, 2022.

483 Rita Lecci, Massimiliano Drudi, Alessandro Grandi, Sergio Creti, Emanuela Clementi: EU Copernicus Marine Service Product
484 User Manual for For Mediterranean Sea Physics Reanalysis, MEDSEA_MULTIYEAR_PHY_006_004, Issue 2.3, Mercator
485 Ocean International, <https://catalogue.marine.copernicus.eu/documents/PUM/CMEMS-MED-PUM-006-004.pdf>, last access:
486 19 May 2023, 2022.

487 Product ref no.3

488 EU Copernicus Marine Service Product: European Seas Gridded L 4 Sea Surface Heights And Derived Variables Nrt, Mercator
489 Ocean International [data set], <https://doi.org/10.48670/moi-00142>, 2023.

490 M-I Pujol, G. Taburet and SL-TAC team.: EU Copernicus Marine Service Quality Information Document for European Seas
491 Gridded L 4 Sea Surface Heights And Derived Variables Nrt,
492 SEALEVEL_EUR_PHY_L4_NRT_OBSERVATIONS_008_060, Issue 8.2, Mercator Ocean International,
493 <https://catalogue.marine.copernicus.eu/documents/QUID/CMEMS-SL-QUID-008-032-068.pdf>, last access: 19 May 2023,
494 2023.

495 M-I Pujol: EU Copernicus Marine Service Product User Manual for European Seas Gridded L 4 Sea Surface Heights And
496 Derived Variables Nrt, SEALEVEL_EUR_PHY_L4_NRT_OBSERVATIONS_008_060, Issue 7.0, Mercator Ocean
497 International, <https://catalogue.marine.copernicus.eu/documents/PUM/CMEMS-SL-PUM-008-032-068.pdf>, last access: 19
498 May 2023, 2022.

499 Product ref no.4

500 S. Simoncelli , P. Oliveri , G. Mattia. SeaDataCloud Mediterranean Sea - V2 Temperature and Salinity Climatology [dataset].
501 <http://dx.doi.org/10.12770/3f8eaace-9f9b-4b1b-a7a4-9c55270e205a> [Accessed on 19 May 2023]

502 Simoncelli Simona, Oliveri Paolo, Mattia Gelsomina, Myroshnychenko Volodymyr, Barth Alexander, Troupin Charles (2020).
503 SeaDataCloud Temperature and Salinity Climatology for the Mediterranean Sea (Version 2). Product Information Document
504 (PIDoc). <https://doi.org/10.13155/77514>

505

506

507